Environmental Science & Technology

pubs.acs.org/est

Article

Metal-Ion Depletion Impacts the Stability and Performance of Battery Electrode Deionization over Multiple Cycles

Le Shi, Evan Newcomer, Moon Son, Vineeth Pothanamkandathil, Christopher A. Gorski, Ahmed Galal, and Bruce E. Logan*

Cite This: *Environ. Sci. Technol.* 2021, 55, 5412−5421

Read Online

ACCESS | Metrics & More | Article Recommendations | Supporting Information

ABSTRACT: Prussian blue hexacyanoferrate (HCF) materials, such as copper hexacyanoferrate (CuHCF) and nickel hexacyanoferrate (NiHCF), can produce higher salt removal capacities than purely capacitive materials when used as electrode materials during electrochemical water deionization due to cation intercalation into the HCF structure. One factor limiting the application of HCF materials is their decay in deionization performance over multiple cycles. By examining the performance of CuHCF and NiHCF electrodes at three different pH values (2.5, 6.3, and 10.2) in multiple-cycle deionization tests, losses in capacity (up to 73% for CuHCF and 39% for NiHCF) were shown to be tied to different redox-active centers through analysis of dissolution of electrode metals. Both copper and iron functioned as active centers for Na^+ removal in CuHCF, while iron was mainly the active center in NiHCF. This interaction of Na^+ and active centers was demonstrated by correlating the decrease in performance to the concentration of these metal ions in the effluent solutions collected over multiple cycles at different pHs (up to 0.86 ± 0.14 mg/L for iron and 0.42 ± 0.17 mg/L for copper in CuHCF and 0.38 ± 0.05 mg/L for iron in NiHCF). Both materials were more stable (<11% decay for CuHCF and no decay for NiHCF) when the appropriate metal salt (copper or nickel) was added to the feed solutions to inhibit electrode dissolution. At a pH of 2.5, there was an increased competition between protons and Na^+ ions, which decreased the Na^+ removal amount and lowered the thermodynamic energy efficiency for deionization for both electrode materials. Therefore, while an acidic pH provided the most stable performance, a circumneutral pH would be useful to produce a better balance between performance and longevity.

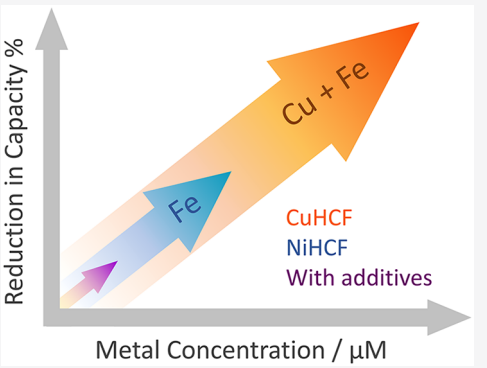

INTRODUCTION

Electrochemical approaches provide alternative methods for deionization to current technologies that use either heat (e.g., thermal distillation) or pressure (e.g., reverse osmosis).[1] These electrochemical systems include electrodialysis,[2] shock electrodialysis,[3] ion concentration polarization,[4] capacitive deionization (CDI),[5−9] and battery electrode deionization (BDI).[10−13] Among these different electrochemical approaches, BDI can achieve a better performance than CDI due to higher capacity of the electrodes for salt removal and improved thermodynamic energy efficiencies.[14] Intercalation electrode materials used in BDI can have higher salt removal capacities than capacitive materials because of their ability to store ions within their crystal lattices.[15] The increased cation storage capacity of intercalation materials reduces energy demands for desalination and avoids parasitic reactions through the use of a smaller voltage window than what is needed to achieve the same desalination extent with capacitive electrode materials.[16−18]

Prussian blue-structured metal hexacyanoferrate (MHCF) materials have been explored for storing electrical charge in applications other than deionization, including rechargeable batteries and biosensors.[10,19−26] MHCF materials have an open-framework crystal structure containing large interstitial sites that allow for the insertion and extraction of a variety of ions, including Li^+, Na^+, K^+, and NH_4^+ in aqueous electrolytes.[27] For example, during electrochemical deionization, an MHCF cathode is reduced, with the insertion of the Na^+ ion into the cathode, and an MHCF anode is oxidized, releasing the preinserted Na^+ ion back into the solution following the half-reaction[12,28,29]

$$NaM[Fe(CN)_6] + xNa^+ + xe^- = Na_{1+x}M[Fe(CN)_6] \quad (1)$$

The MHCF electrodes can intercalate Na^+ (3.6 Å hydrated radius) or other cations with sizes similar to those of the interstitial sites, such as 3.2−4.6 Å for copper hexacyanoferrate

Received: December 21, 2020
Revised: March 6, 2021
Accepted: March 16, 2021
Published: March 30, 2021

(CuHCF).[27,30,31] The specific structure of these materials is well known and reported in previous literature.[26,27,32] Nickel hexacyanoferrate (NiHCF) and CuHCF have very similar lattice parameters, but the capacity performance of these MHCF electrodes decays over time at rates which are dependent on the operation conditions (e.g., applied current density, contained electrolyte in a battery, or continuous flow in the deionization process), cations in the electrolyte (e.g., K^+ or Na^+), and the specific metal in the MHCF (e.g., copper or nickel). For example, the capacity of the CuHCF cathode declined by only 17% compared to its original capacity after 40,000 cycles in batteries using a KNO_3 (1 M) electrolyte at 1.02 A/g (17 C rate).[33] However, in CuHCF electrodes with Na^+-based electrolytes, the performance declined by 23% after 500 cycles at 0.5 A/g[27] and by 43% after only 50 cycles in sodium-ion batteries at 0.02 A/g.[34] The pH of the electrolytes in these battery studies ranged from 1 to 4.[27,32,35] In electrochemical deionization tests, which typically contain feed waters with pH values near 7, the electrode performance decays more rapidly. CuHCF electrodes lost 53% of their capacity after 50 cycles using 20 mM NaCl as brackish water at 0.1 A/g (5 A/m^2),[11] and NiHCF electrodes lost 75% of their capacity after 120 cycles using solutions with Mg^{2+} and Ca^{2+} cations at 0.05 A/g (2.5 A/m^2).[36] The reasons for ion-storage capacity changes for MHCF electrodes need to be better understood in order to improve their stability for use in electrochemical deionization systems.

The operating conditions in BDI deionization tests with MHCF electrodes, where the electrolyte (brackish water or seawater) has a near-neutral pH and there is a continuous flow of this feed solution through the cells, are much different than those for batteries which use a completely contained acidic electrolyte. To investigate the effects resulting from the specific metal used in the MHCF electrodes and the feed solution pH conditions on salt removal capacities in deionization applications compared to those used for batteries, the performance and stability of CuHCF and NiHCF electrodes were examined in BDI flow cells as a function of solution pH (2.5, 6.3, and 10.2) under continuous flow conditions. The overall performance was evaluated using several metrics including the specific adsorption capacity (SAC) of Na^+ ions, charge efficiency, and thermodynamic energy efficiency (TEE). Stability was investigated by examining changes in the ion capacity, concentrations of metals (copper, nickel, and iron) in effluent solutions over multiple cycles, and the impact of adding metal salts into feed solutions to better simulate the conditions of a contained electrolyte in order to minimize dissolution of the electrodes. The Na^+ removal kinetics by CuHCF and NiHCF electrodes was analyzed using a scan-rate-dependent CV method.

MATERIALS AND METHODS

Battery Electrode Fabrication. CuHCF and NiHCF powders were synthesized using a coprecipitation method as previously reported.[10−12] $K_3[Fe(CN)_6]$ (0.05 M, 0.5 ml/min, J.T. Baker) and either $Cu(NO_3)_2$ or $Ni(NO_3)_2$ (0.1 M, 0.5 ml/min, Sigma-Aldrich) were added into deionized water with vigorous stirring at room temperature. The precipitates were washed by centrifugation over several cycles and dried overnight in a vacuum oven (70 °C). The produced powders (CuHCF or NiHCF) were ground and mixed with carbon black (Vulcan XC72R, Cabot, average particle size = 50 nm) and polyvinylidene fluoride (Kynar HSV 900, Arkema Inc.) in a mass ratio of 8:1:1 in 1-methyl-2-pyrrolidinone (NMP, Sigma-Aldrich) (28.8:3.6:3.6 mg in 0.5 ml for one piece). The slurry was drop cast onto a carbon cloth (with an area of 7 cm^2, a thickness of 0.356 mm, and a density of 1.5 g/cm^3, AvCarb 1071 HCB, AvCarb Material Solutions). The counter electrode for the preconditioning and cyclic voltammetry (CV) test was prepared by the same drop-casting method except for activated carbon (AC) used in place of CuHCF or NiHCF powders. The coated samples were dried on a hotplate at 70 °C for 3 h and then in a vacuum oven at 70 °C overnight.

Electrode Characterization. The surface morphology of the MHCF electrodes was analyzed using scanning electron microscopy (SEM, Verios G4, Thermo Fisher Scientific). The elemental atomic ratio of each metal ion was analyzed using energy-dispersive X-ray spectroscopy (EDS). The CV profiles with feed solutions (1 M NaCl) at three different pHs (2.5, 6.3, and 10.2) were recorded in a three-electrode system at six different scan rates (1, 2, 3, 5, 10, and 20 mV/s) with CuHCF or NiHCF as the working electrode, AC as the counter electrode, and a Ag/AgCl reference electrode (3 M NaCl, +0.209 V with respect to a SHE) using a potentiostat (VNP3, Bio-Logic). In theory, the voltammetric response follows a power-law relationship of measured current with the scan rate according to the following eq[37−40,65]

$$i = av^b \tag{2}$$

where i is the measured peak current (mA), v is the scan rates (mV/s), and both a and b are adjustable parameters. For a typical intercalation process which is limited by a semi-infinite linear diffusion process, the peak current i varies with $v^{1/2}$ (b = 0.5); for a surface-controlled process, such as adsorption, it varies with v (b = 1).

Electrode Conditioning. Before deionization performance tests, the potentials of the two MHCF electrodes were adjusted to different potentials to optimize their performance relative to Na^+ removal. The CuHCF electrodes were set to 0.4 V (Na^+ enriched) and 1.0 V (Na^+ depleted) (vs Ag/AgCl in 3 M NaCl) with a three-electrode system containing the working (CuHCF), counter (AC), and reference (Ag/AgCl in 3 M NaCl) electrodes and 1 M NaCl as the electrolyte. A constant current of ±10 A/m^2 was applied until the predetermined cutoff voltage (0.4 and 1.0 V) was reached. Similarly, the potentials of the two NiHCF electrodes were adjusted to 0.1 V (Na^+-enriched) and 0.7 V (Na^+-depleted) (vs Ag/AgCl in 3 M NaCl) in a comparable system.

Deionization Experiments. The BDI performance was tested in a lab-made flow cell system constructed as previously reported.[10−12] The cell had two chambers (with 7 cm^2 effective cross-sectional area), each containing a CuHCF or NiHCF electrode as the working and counter electrodes, separated by an anion-exchange membrane (AEM, 106 ± 1 μm thick with an ion-exchange capacity of 1.85 mmol/g, Selemion AMV, Asahi Glass) (Figure 1).[41] The Na^+-enriched CuHCF or NiHCF electrode was used as the anode and the Na^+-depleted CuHCF or NiHCF electrode as the cathode. A fabric spacer (0.28 mm thick and 33% porosity; Sefar Nitex, 06-210/33) was placed in between the electrode and AEM to distribute the solution evenly on the electrode surface. The feed solution of synthetic brackish water (50 mM NaCl) at a set pH (2.5, 6.3, and 10.2 adjusted by adding H_2SO_4 and NaOH) was continuously fed to the BDI cell at a flow rate of 0.5 mL/min (no recycle). A set constant current of ±10 A/m^2 was applied between the anode and the cathode at a voltage

https://doi.org/10.1021/acs.est.0c08629
Environ. Sci. Technol. 2021, 55, 5412−5421

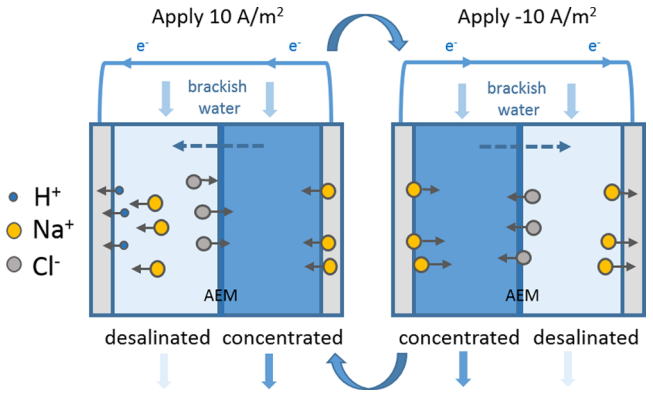

Figure 1. Schematic of a BDI flow cell using CuHCF or NiHCF electrodes in two channels separated by an AEM when a sufficient concentration of H^+ is present in the solution.

window of ±0.6 V using a potentiostat (VNP3, Bio-Logic). The conductivity of the effluent was measured using flow-through conductivity electrodes (ET908 Flow-Thru Conductivity Electrode, eDAQ) located at each outlet and converted to a NaCl concentration using a linear calibration curve. Each pair of electrodes was used in only one type of feed solution.

Electrode Stability Test. The electrode stability test conditions were the same as those used in deionization experiments except that the tests were conducted for a total of 52 cycles (Figures S1 and S2). The effluents from the two channels were collected in one container without recycling to measure total metal dissolution during the tests conducted at different pHs. The ion composition in the effluents was measured by inductively coupled plasma optical emission spectroscopy (ICP-OES, ICAP 7400, Thermo Fisher). Control experiments (no electrode preconditioning or current) were conducted by immersing one piece of CuHCF or NiHCF electrode in different pH solutions containing 50 mM NaCl with the same volume of 250 mL for 10 h. The total volume of effluent collected after 52 cycles varied depending on the solution pH due to differences in cycle durations. The samples were diluted four times with 2% HNO_3 solution and stored at 4 °C before analysis.

Calculations. The deionization performance was examined in terms of specific adsorption capacity, specific capacity, charge efficiency, cycling efficiency, and thermodynamic energy efficiency. Specific adsorption capacity (SAC, mg of Na^+ per gram of electrode, mg g^{-1}) was calculated as

$$\mathrm{SAC} = \frac{M_{\mathrm{Na}} \int_0^{T_c} C_{\mathrm{Na}} \mathrm{d}t}{E_{\mathrm{mass}}} \tag{3}$$

where T_c is the charging or cycling time, C_{Na} the moles of Na^+ removed in the desalinated chamber, M_{Na} the molecular weight of Na^+, and E_{mass} the electrodeactive material mass. Specific capacity (SC, mA h g^{-1}) was calculated as

$$\mathrm{SC} = \frac{\int_0^{T_c} I \mathrm{d}t}{E_{\mathrm{mass}}} \tag{4}$$

where I is the applied current. Charge efficiency (Λ, %) was calculated as the ratio of the charge consumption for Na^+ removal to the total charge put into the electrode over a full cycle

$$\Lambda = \frac{F \int_0^{T_c} C_{\mathrm{Na}} \mathrm{d}t}{\int_0^{T_c} I \mathrm{d}t} \times 100 \tag{5}$$

where F is Faraday's constant (96,485 C mol^{-1}). Cycling efficiency (CE, %) was calculated as

$$\mathrm{CE} = \frac{\sum T_{\mathrm{D}}}{\sum T_c} \times 100 \tag{6}$$

where T_D is the discharge time and T_C is the charging time. The charge and discharge times are the time taken for the voltage to increase from −0.6 to 0.6 V or decrease from 0.6 to −0.6 V at a constant current, ±10 A m^{-2}. Energy consumption (E_C, kW h m^{-3}) was calculated as

$$E_{\mathrm{C}} = \frac{\int_0^{T_s} VI \mathrm{d}t}{J_{\mathrm{W}}} \tag{7}$$

and energy recovery (E_R, kW h m^{-3}) was calculated as

$$E_{\mathrm{R}} = \frac{\int_0^{T_f} VI \mathrm{d}t}{J_{\mathrm{W}}} \tag{8}$$

where T_f is the beginning of the first half-cycle when the flows are switched (−0.6 to 0 V when 10 A m^{-2} is applied or 0.6 to 0 V when −10 A m^{-2} is applied). T_s is the rest of the half-cycle until the direction of applying current is switched and J_w is the water flux during operation (volume of desalinated water during T_f and T_s). During the ion adsorption step (T_s), the voltage (V) and the current (I) have the same sign (either positive or negative), meaning that this step consumes energy. However, during the ion desorption step (T_f), the voltage (V) and the current (I) have different signs since ions are spontaneously released so that this step recovers energy. Energy recovery was calculated when the direction of the applied current was switched until the cell voltage reached 0 V. Thermodynamic energy efficiency (TEE, %) was calculated as

$$\mathrm{TEE} = \frac{\Delta g}{E_c - E_{\mathrm{R}}} \times 100 \tag{9}$$

The specific Gibbs free energy of separation (Δg, kW h m^{-3}) was calculated as

$$\Delta g = 2RT \left\{ \frac{C_0}{\gamma} \ln\left[\frac{C_0 - \gamma C_{\mathrm{D}}}{C_0(1-\gamma)}\right] - C_{\mathrm{D}} \ln\left[\frac{C_0 - \gamma C_{\mathrm{D}}}{C_{\mathrm{D}}(1-\gamma)}\right] \right\} \tag{10}$$

where R is the ideal gas constant equal to 8.314 J mol^{-1} K^{-1}, T is the absolute temperature (room temperature 298 K), C_0 is the feed concentration, C_D is the product water concentration at a steady state, and γ is the water recovery calculated as

$$\gamma = \frac{V_{\mathrm{D}}}{V_{\mathrm{D}} + V_{\mathrm{C}}} \times 100 \tag{11}$$

where V_D is the volume of desalinated water and V_C is the volume of concentrated water. In all experiments, the flow rates of both chambers were the same, so the water recovery was fixed at γ = 50%. All of these performance metrics were calculated based on the second charge and discharge cycles with all experiments conducted in duplicate with a pair of new electrodes for each test.

https://doi.org/10.1021/acs.est.0c08629
Environ. Sci. Technol. 2021, 55, 5412−5421

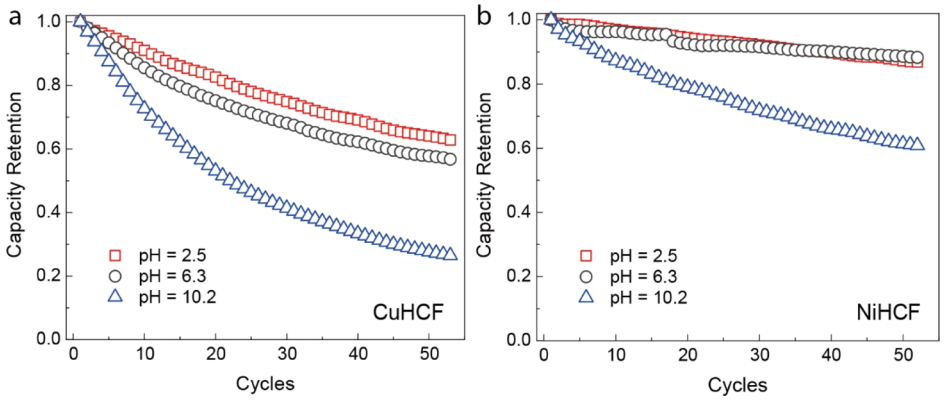

Figure 2. Capacity retention of (a) CuHCF and (b) NiHCF electrodes over 52 cycles in the BDI flow cell with 50 mM NaCl feed solution with different pHs (2.5, 6.3, and 10.2). A constant current of ±10 A/m^2 was applied in the voltage window of ±0.6 V with a flow rate of 0.5 mL/min.

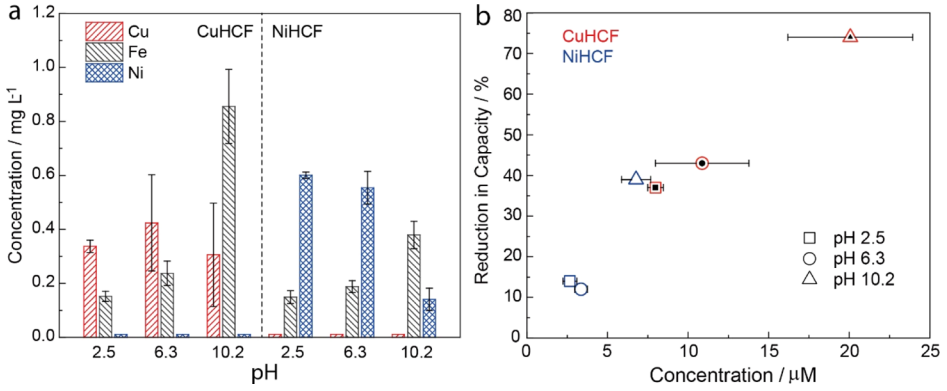

Figure 3. (a) Metal-ion concentration (mg/L) in effluents collected over 52 cycles of deionization tests with CuHCF or NiHCF electrodes with a 50 mM NaCl feed solution in different pHs (2.5, 6.3, and 10.2). A constant current of ±10 A/m^2 was applied in the voltage window of ±0.6 V with a flow rate of 0.5 mL/min. (b) Relationship between the capacity reduction of CuHCF and NiHCF electrodes at different pHs (2.5, 6.3, and 10.2) and the concentration (μM) of metal ions in effluents (Fe only for the NiHCF electrode and the sum of Fe and Cu for the CuHCF electrode). Error bars show the standard deviation between replicates using different pieces of electrodes. A filled symbol was used to indicate the sum of Cu and Fe, and the empty symbol was for only Fe.

RESULTS AND DISCUSSION

Electrode Stability in Different Feed Solutions. The CuHCF electrodes had a much greater reduction in capacity retention than the NiHCF electrodes after 52 deionization cycles at all three pH conditions (Figure 2). The CuHCF electrodes retention decreased by 43% using the pH = 6.3 solution by the end of the process compared to 37% with the acidic solution (pH = 2.5). Under alkaline conditions (pH = 10.2), the CuHCF performance decayed even faster with a 73% loss of capacity retention after the 52 cycles. In contrast, the NiHCF electrodes had a reduction of only 12% at pH = 6.2 and 14% at pH = 2.5. The NiHCF solutions also showed a large change in stability with the alkaline solution, with a decay of 39% at a pH of 10.2 solution (Figure 2).

Metal concentrations measured in the effluents collected from both sides of the cell following the 52 deionization cycles showed a clear trend of increase in dissolved iron concentrations with increased pH for both electrode materials (Figures 3a and S3a). For the CuHCF electrodes, as the feed solution pH increased, the dissolved iron concentration increased slightly from 0.15 ± 0.02 mg/L at pH = 2.5 to 0.24 ± 0.04 mg/L at pH = 6.3, consistent with the slightly decreased performance at these two pHs. In the pH = 10.2 solution, the dissolved iron increased to 0.86 ± 0.14 mg/L, which was consistent with the large drop in performance of this material (Figure 2a). The iron signal was assumed to be from $Fe(CN)_6^{3-}$ and $Fe(CN)_6^{4-}$ rather than from free Fe ions due to the tight binding of the CN^- to the Fe^{3+} or Fe^{2+}.[42,43] Copper was also measured in the effluents, with the lowest concentration of 0.31 ± 0.19 mg/L measured for the highest loss of retention (73%) at pH = 10.2 and the highest concentration of 0.42 ± 0.17 mg/L at pH = 6.3. All the metal ions depleted due to chemical reactions were much smaller under all three pH conditions compared to those with the applied current in the BDI cycling test (Figure S3a).

The decay of capacity retention performance of the NiHCF electrodes was correlated with a loss of iron from the electrodes after the long-term cycling tests. In the tests at the two lower pH conditions, the iron concentrations were low with only a slightly higher increase in iron at pH = 6.3 (0.19 ± 0.02 mg/L) compared to pH = 2.5 (0.15 ± 0.02 mg/L) (Figure 3a), consistent with a similar change in capacity retention performance for the NiHCF electrodes (Figure 2b). A much larger increase in the concentration of iron was measured at the relatively high pH = 10.2 of 0.38 ± 0.05 mg/L, which coincided with a substantial reduction in NiHCF performance at that pH. While nickel was measured in the solutions at all three pHs, the lowest nickel concentration was found in the alkaline solutions indicating improved stability of nickel at pH = 10.2 compared to the CuHCF electrodes. In

https://doi.org/10.1021/acs.est.0c08629
Environ. Sci. Technol. 2021, 55, 5412−5421

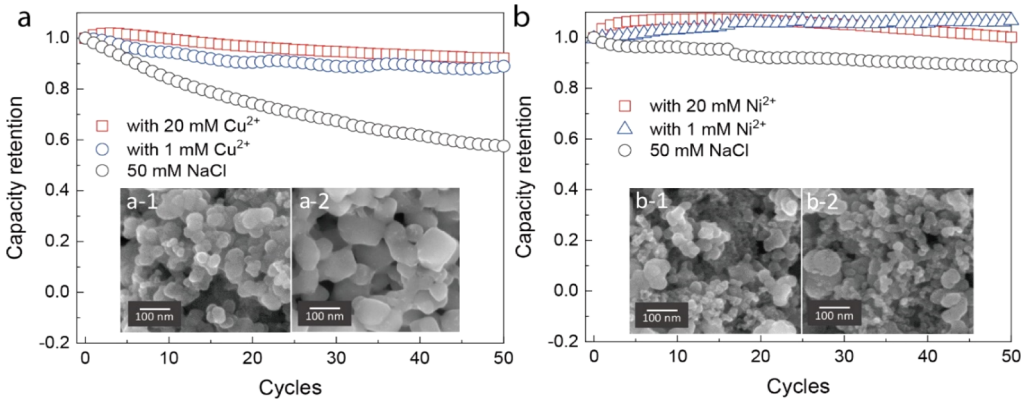

Figure 4. Capacity retention of (a) CuHCF and (b) NiHCF electrodes with additives of 20 and 1 mM $Cu(NO_3)_2$ and 20 and 1 mM $Ni(NO_3)_2$, respectively, in a 50 mM NaCl (pH = 6.3) feed solution over 50 cycles in the BDI flow cell. A constant current of ±10 A/m^2 was applied in the voltage window of ±0.6 V with a flow rate of 0.5 mL/min. Curves for 50 mM NaCl are the same as in Figure 2 at pH = 6.3 condition for CuHCF and NiHCF electrodes. Insets show the SEM images of the fresh active material ((a-1) CuHCF and (b-1) NiHCF) and the active material after cycling in 50 mM NaCl (pH = 6.3) ((a-2) CuHCF and (b-2) NiHCF).

contrast to the loss of copper in CuHCF electrodes, the NiHCF electrodes showed a large amount of nickel dissolution at pH = 2.5 (0.6 ± 0.01 mg/L) and 6.3 (0.55 ± 0.06 mg/L) solutions. However, this higher loss of nickel from the electrodes at this low pH did not result in a greater decay in performance for the NiHCF electrodes, which indicated that nickel was not the reactive center for Na^+ intercalation in the NiHCF electrodes.

The concentrations measured in the effluents from multiple-cycle (long-term) BDI tests for the three metals (iron, copper, and nickel) (Figures 3 and S3) suggest different Na^+ ion interactions with copper in the CuHCF electrodes compared to those with nickel in the NiHCF electrodes. For both electrodes, the highly increased dissolution of iron into the solution at pH = 10.2 explained the highly increased losses in capacity retention compared to the other two pHs due to the increased chemical decomposition.[42] The main differences between the two electrodes were seen at the lower pHs based on the measured concentrations of copper and nickel in the effluents. For the NiHCF electrodes, there was a high concentration of nickel in the effluent but the decrease in the performance was less than that for the CuHCF electrodes. It was found that with a similar iron depletion for CuHCF and NiHCF electrodes in acidic and neutral pHs, the capacity reduction for the CuHCF electrode was much larger than that for the NiHCF electrode (Figure S3b). For example, the iron depletion was 2.71 ± 0.34 μM from CuHCF and 2.66 ± 0.42 μM from the NiHCF electrode under acidic conditions, while the capacity reduction was 37% for the CuHCF electrode but only 14% for the NiHCF electrode. Therefore, considering that there was similar iron depletion from both electrodes, the observed decrease in performance of the CuHCF electrode was concluded to be associated with the loss of copper at the lower pH conditions. A linear relationship was found between the capacity reduction using the sum of copper and iron concentrations in the effluents for the CuHCF electrodes but only iron concentrations for NiHCF electrodes (Figure 3b). The opposite trend for the copper and nickel concentrations relative to the capacity retention performance suggested that copper was active with Na^+ intercalation but nickel was not directly interacting with Na^+. Previous studies on batteries (using contained electrolytes) have suggested that the performance of NiHCF electrodes in aqueous divalent electrolytes was linked to the dissolution of Ni^{2+}.[36,44] Following a noticeable initial decay in retention capacity in the battery, the subsequent performance was shown to be stable due to the elevated concentration of nickel in the contained electrolyte.[44] This suggested that the observed decays in performance here in the deionization process were associated with the continued loss of electrodes under continuous flow conditions.

To test the importance of the concentrations of copper or nickel ions in the electrolytes, lower concentrations of these metals were added to the feed solutions. When $Cu(NO_3)_2$ was added to the feed solution containing 50 mM NaCl (pH 6.3) with CuHCF electrodes, the capacity retention decay was only 8% with 20 mM $Cu(NO_3)_2$ and 11% with 1 mM $Cu(NO_3)_2$ after 50 cycles compared to its initial capacity (Figure 4). For the NiHCF electrodes, when 20 or 1 mM $Ni(NO_3)_2$ was added to the feed solution, there was essentially no decay in performance over time. These lower concentrations of additives rule out possible impacts of the intercalation of Cu^{2+} ions (4.2 Å) and Ni^{2+} ions (4.0 Å) influencing these results.[27,30,31] In both cases, there was a slight increase in capacity retention that could have occurred for different reasons. In the case of CuHCF electrodes, the limited dissolution of copper provided more reactive active centers for Na^+ intercalation and prevented the collapse of the lattice structure. For NiHCF electrodes, the presence of nickel in the solution could reduce the dissolution of nickel and help maintain the integrity of the lattice structure for improved stable performance over multiple cycles. From these results, we can infer that a critical factor in the decrease of capacity performance was the loss of copper or nickel from the electrodes. The dissolution of copper and nickel caused a collapse in the lattice structure, resulting in the loss of iron, which further contributed to the overall loss in performance. In batteries, the loss of the electrode metals results in saturation of the solutions and thus enables greater stability of the capacity retention relative to performance.[44] It is important to mention that the addition of background ions was not designed as a strategy for improving the performance stability but to prove the hypothesis that metal depletion was one of the key reasons for capacity reduction in BDI systems using MHCF electrodes. The results obtained here demonstrated a reason for the decreased performance and therefore that new

https://doi.org/10.1021/acs.est.0c08629
Environ. Sci. Technol. 2021, 55, 5412−5421

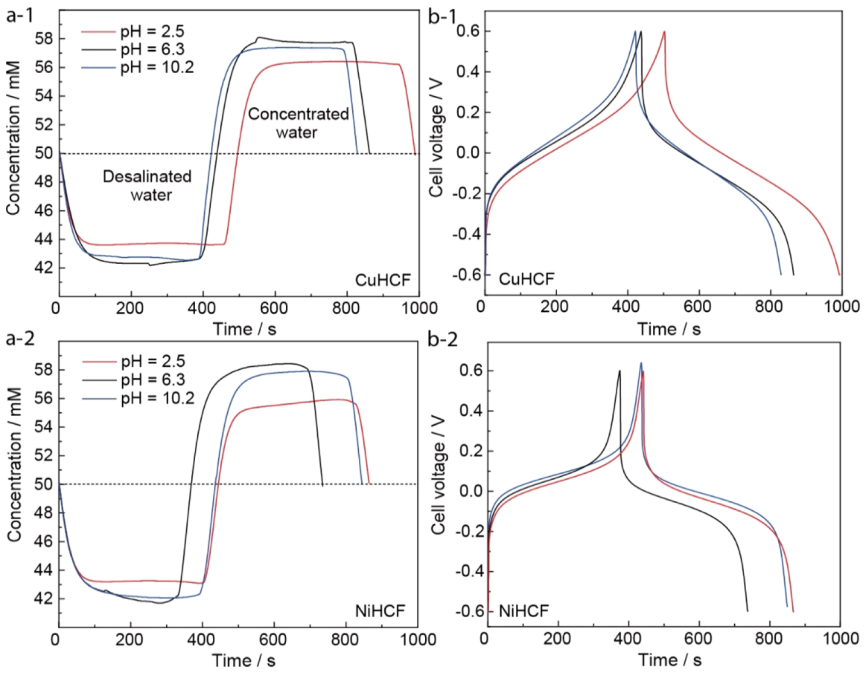

Figure 5. (a) Representative effluent concentration profiles and (b) cell voltages of the CuHCF and NiHCF electrodes for one complete charge and discharge cycle with 50 mM NaCl feed solution with different pHs (2.5, 6.3, and 10.2). A constant current of ±10 A/m^2 was applied in the voltage window of ±0.6 V with a flow rate of 0.5 mL/min.

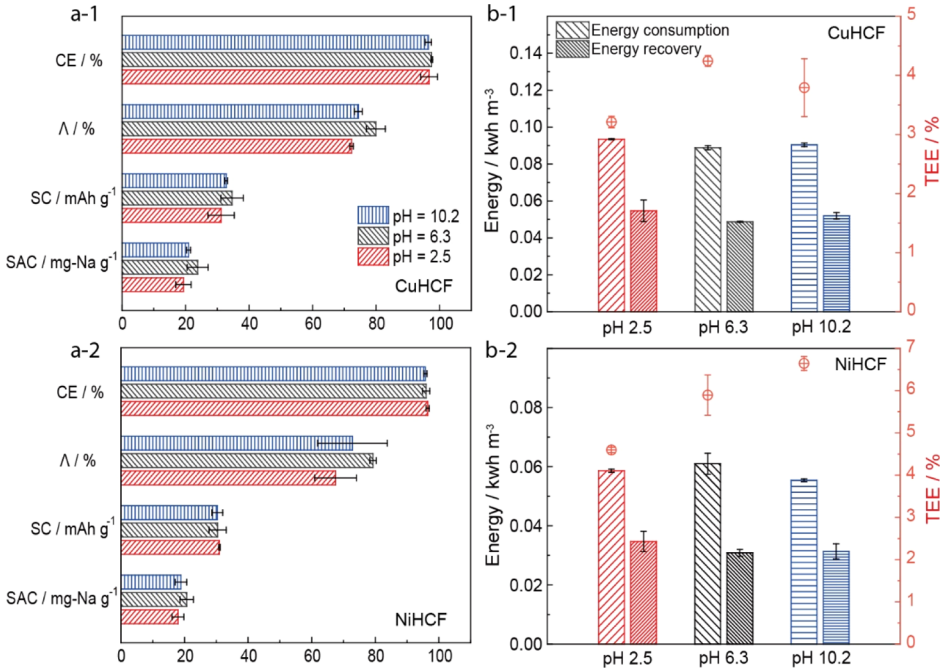

Figure 6. (a) Specific adsorption capacity (SAC, mg-Na/g), specific capacity (SC, mA h/g), charge efficiency (Λ, %), and cycling efficiency (CE, %) and (b) energy consumption (kW h/m^3) and recovery (kW h/m^3) and thermodynamic energy efficiency (TEE, %) of both CuHCF and NiHCF electrodes with 50 mM NaCl feed solution of different pHs (2.5, 6.3, and 10.2). The data for calculations were collected from the second complete charge and discharge cycle. Error bars show the standard deviation between replicates using different pieces of electrodes.

approaches are needed for improving the electrode stability in the electrochemical deionization process. The conditions which produced stability in batteries using a contained electrolyte under acidic solution conditions cannot be adopted even though similar electrode materials are used in these two fields.

The SEM images showed that the as-synthesized CuHCF and NiHCF powders consist of micrometer-size particles (Figure S4) composed of smaller particles 10−60 nm in size (Figure 4). A higher number of cubic-shaped particles having larger sizes were observed on the CuHCF sample after cycling in 50 mM NaCl (pH 6.3) with and without the Cu-ion additives (Figures 4a and S4b,c). Such changes in the cubic-shaped morphology following cycling tests have been previously reported in studies using CuHCF electrodes in Ca- and Zn-ion batteries.[45−47] The morphological trans-

https://doi.org/10.1021/acs.est.0c08629
Environ. Sci. Technol. 2021, 55, 5412−5421

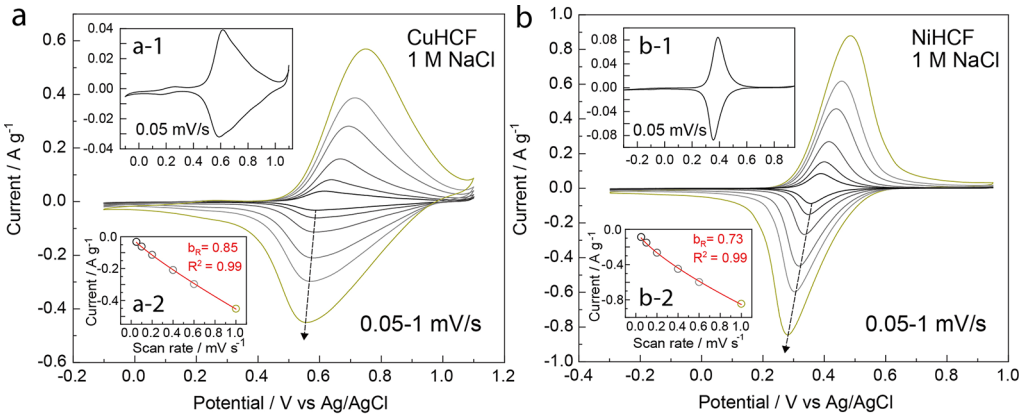

Figure 7. CV curves of the (a) CuHCF and (b) NiHCF electrodes measured at various scan rates (0.05−1 mV/s) in 1 M NaCl (pH 6.3). CV curves of CuHCF and NiHCF electrodes obtained at 0.05 mV/s are presented separately in (a-1) and (b-1), respectively, with the same axis as (a) and (b). Insets of (a-2) and (b-2) show the results to determine the b-values of reduction peaks by CuHCF and NiHCF electrodes, respectively, where the red lines are regression models to fit the experimental data. Current densities were normalized by the active material loading mass.

formation of CuHCF electrodes via reaction with Na^+ ions might be due to the substitution of Cu ions by Na ions in substitutional as well as in interstitial sites.[45] For NiHCF electrodes, there were no obvious particle shape and size changes observed after cycling in 50 mM NaCl (pH 6.3) with and without Ni-ion additives. The morphology changes also indicated that the reactive center for CuHCF and NiHCF electrodes might be different for Na^+ intercalation in this process. The atomic ratios of Cu:Fe in the CuHCF electrode and Ni:Fe in the NiHCF electrode collected under different conditions were calculated based on the relative atomic percentage of each metal ion through SEM−EDS analysis (Table S1). The abundance of Cu and Ni was normalized to one Fe unit. For the CuHCF electrode, this ratio was changed from 1.21:1 (fresh electrode) to 1.14:1 after cycling in 50 mM NaCl (pH 6.3) and to 1.69:1 after cycling with added Cu ions to the solution. The atomic ratios for Ni:Fe in the NiHCF electrode changed from 1.45:1 to 1.52:1 after cycling in 50 mM NaCl (pH 6.3) and then to 1:44:1 after cycling with background Ni ions. The increased ratio of Cu:Fe after cycling with additives would be expected from the possible residual Cu on the surface of the material. However, as the atomic percentage of Na or K was also changed for the samples under different conditions, it was difficult to reach a clear conclusion about the fate of the metals relative to retention in the materials or loss into the solution from these studies.

Deionization Performance. Adjustment of the pH of the feed solution appeared to have an impact on the internal resistance of the BDI cell based on the potential drop between charge and discharge cycles as well as on salt adsorption in terms of the deionization performance.[48] The potential of the electrode instantaneously decreases as the direction of the current changed under constant current conditions due to the internal resistance of the cell.[49] The potential drop (or Ohmic drop) in the interval between the charge and discharge cycles (Figure S5) was smaller for both CuHCF and NiHCF electrodes in pH 2.5 (0.18 V for CuHCF and 0.34 V for NiHCF) and pH 10.2 (0.21 V for CuHCF and 0.38 V for NiHCF) conditions compared to the pH 6.3 condition (0.25 V for CuHCF and 0.40 V for NiHCF). This smaller potential drop of the system with acidic and basic feed solutions was likely due to the increased conductivity of the feed solution along with the adjustment of the solution pH.

For both CuHCF and NiHCF electrodes, a 50 mM NaCl solution was desalinated by 12% (to 44 mM) using the acidic feed solution, which was less than that using the neutral (16%, to 42 mM) or basic (14%, to 43 mM) feed solutions (Figure 5a). This result was a consequence of lower salt adsorption (Figures 5a and S6) at the lowest pH = 2.5 (SAC = 19.4 ± 2.4 mg-Na/g for CuHCF and 17.9 ± 1.9 mg-Na/g for NiHCF) (Figure 6a), compared to the higher near-neutral pH = 6.3 (SAC = 23.8 ± 3.2 mg-Na/g for CuHCF and 20.7 ± 2.1 mg-Na/g for NiHCF) conditions. A smaller charge efficiency was observed under acidic conditions for CuHCF (Λ = 72.3 ± 0.5%) and NiHCF (Λ = 67.5 ± 6.5%) compared to that under the neutral condition (79.9 ± 2.9% for CuHCF and 79.3 ± 1.1% for NiHCF). The smaller SAC and Λ indicated the possible occurrence of side reactions of co-intercalation of protons into the electrode, the hydrogen evolution reaction (HER) and the oxygen evolution reaction (OER), which would consume a portion of the charge and therefore do not contribute to the removal of Na^+ from the solution.[14,50,51] As shown in studies on aqueous batteries, the use of neutral pH electrolytes generally show higher operating voltages than acidic or alkaline electrolytes, which is attributed to the larger HER and OER overpotentials in the neutral electrolytes.[52] The cycling efficiency for both electrodes under all three conditions was high (CE > 94%), indicating nearly identical duration time for charging and discharging cycles for each condition.[12]

The thermodynamic energy efficiency (TEE) of different conditions based on the fraction of the consumed energy utilized for sodium removal was the lowest in acidic solutions for both electrode materials. For example, the TEE was 3.2 ± 0.1% for CuHCF and 4.5 ± 0.05% for NiHCF under acidic conditions, and it increased to 4.2 ± 0.1% for CuHCF and 5.9 ± 0.5% for NiHCF under near-neutral conditions (Figure 6). The smaller TEE obtained in the acidic solution indicated a less energy-efficient deionization performance, which might be due to the intercalation competition between the protons and Na^+ ions. The proton intercalation can be observed from the redox peaks in the CV curve using dilute HCl acid with a pH of 2.5 for both CuHCF and NiHCF electrodes (Figure S7). Protons can insert into the CuHCF and NiHCF cathodes before Na^+ ions because they have a smaller size (2.82 Å for H_3O^+) and diffuse faster than Na^+ ions.[31,50,53] It was also reported that a high number of protons in the host electrode

https://doi.org/10.1021/acs.est.0c08629
Environ. Sci. Technol. 2021, 55, 5412−5421

material may increase the diffusion barrier for intercalating cations and subsequently block intercalation channels.[54]

Kinetic Analysis for Sodium Removal. The Na^+ removal kinetics of CuHCF and NiHCF electrodes in this BDI system was investigated using a scan-rate-dependent CV test (Figure 7), commonly applied in the battery field, to investigate the ion storage mechanism. The b values obtained by fitting eq 2, using the reduction stages in the scan rates of 0.05−1 mV/s, were greater than 0.5 for both materials, with 0.85 for CuHCF and 0.73 for NiHCF electrodes (Figure 7a-2,b-2). Values of $b > 0.5$ suggest that either surface-controlled processes contributed to Na^+ removal or a fast Faradaic process with minimal diffusion limitations occurred due to the small sizes of the active-material particles.[38,55−57] The b values of electrode materials after BDI cycling tests (50 mM NaCl pH 6.3) were also analyzed, with $b = 0.91$ for the CuHCF electrode and $b = 0.67$ for the NiHCF electrode (Figure S8). The reasons for these changes in b value were not clear. Also, a purely capacitive effect should show a rectangular CV (Figure S9) rather than the clear presence of sharply defined redox peaks here. These various results suggesting different mechanisms and the contrasting shapes of the CV curves indicated that further and more detailed investigations are needed for understanding these results relative to the Na^+ removal process as the Prussian blue materials are expected to be mainly controlled by diffusion-controlled processes in the bulk phase materials.

Different reactive centers for Na^+ intercalation in these two materials were further supported by the different CV curves obtained for the CuHCF and NiHCF electrodes (Figure 7a-1,b-1). The capability for Na^+ intercalation with MHCF electrodes was attributed mainly to the reaction of Fe (II) ↔ Fe (III), which can be seen by the redox peaks with an average potential ($E_{1/2}$) of 0.60 V vs Ag/AgCl in pH 6.3 (1 M NaCl) for CuHCF electrodes (Figure 7a-1) and $E_{1/2}$ of 0.37 V for NiHCF electrodes with a scan rate of 0.05 mV/s (Figure 7b-1). It was observed here that both the copper and iron in CuHCF electrodes were redox-active centers because for this material there is another pair of redox peaks with $E_{1/2}$ of 0.23 V due to the reaction of Cu (I) ↔ Cu (II) over the larger potential window (Figure 7a-1).[58−61] The potential of both the cathode and the anode could shift during the deionization process to the region for the reaction of Cu (I) ↔ Cu (II) and thus this shift further degrades the capacity retention of the CuHCF electrodes due to a cubic to tetragonal solid-state phase transition that accompanies the Cu(II) reduction.[58,59] In NiHCF electrodes, the Ni ion was relatively inactive in the potential window (Figure 7b-1) and therefore only iron ions were active for Na^+ intercalation with this material.

Outlook. A higher pH feed solution and the operation of the BDI system under continuous flow conditions led to a decrease in the electrode capacity retention of cations and consequently a reduction in deionization performance. In batteries that use MHCF materials, electrode dissolution can occur, but the extent of loss of material is limited by saturation of the metals in the contained electrolytes. Operation of the BDI under continuous flow conditions resulted in continuous dissolution of these materials and relatively rapid decay of the CuHCF and NiHCF electrodes over multiple cycles.[44] This link between dissolution and performance was shown by adding copper or nickel salts to the feed solutions as that minimized (CuHCF electrodes) or prevented decay (NiHCF electrodes) in capacity retention. The use of a low pH feed solution minimized the dissolution of electrode materials and maintained more stable capacity retention, but it did not completely prevent a decay in performance. The feed solution conditions also impacted the internal resistances and contributed to the generation of side reactions such as co-intercalation of protons (at low pH) in addition to Na^+, dissolved oxygen reduction, and HER/OER on the surface of the electrodes.

The Na^+ removal kinetics by CuHCF and NiHCF electrodes were found to be a function of either a surface-controlled process or a fast Faradaic process that had no diffusion limitation due to the small-size particles. As a result, the design of the electrode materials for the BDI system should take advantage of the fast reaction kinetics from the surface-controlled process and the high ion removal capacity from the intercalation process. Different reactive centers were found for Na^+ intercalation for CuHCF and NiHCF electrodes. For CuHCF electrodes, Na^+ intercalation involved the reaction of Cu (I) ↔ Cu (II) in addition to the single-phase reaction of Fe (II) ↔ Fe (III). The dual redox-active centers in CuHCF electrodes could therefore provide a higher Na^+ adsorption capacity than the electrodes with a single redox-active center such as NiHCF, if the copper in the electrodes could be better stabilized over time. The general electrochemical behavior of CuHCF is known to be more complex than that of other Prussian blue analogues, and many factors can influence the activity of Cu(II) and Cu(I), such as the effect of specific cations in the feed solution, crystal vacancies, and water content of the CuHCF framework.[26,60,62−64] An improved understanding of different cation interactions with the copper and nickel metals in these electrodes will be needed to improve the stability of these electrodes for brackish water deionization applications.

■ ASSOCIATED CONTENT

Supporting Information

The Supporting Information is available free of charge at https://pubs.acs.org/doi/10.1021/acs.est.0c08629.

Cell voltage profiles recorded for multiple cycles, control experiment for metal concentration in the effluent solution, cell voltage profiles during the energy recovery step, CV curves at various scan rates of the carbon cloth electrode, and SEM−EDS results of electrodes under different conditions (PDF)

■ AUTHOR INFORMATION

Corresponding Author

Bruce E. Logan − *Department of Civil and Environmental Engineering, The Pennsylvania State University, University Park, Pennsylvania 16802, United States;* orcid.org/0000-0001-7478-8070; Phone: +1-814-863-7908; Email: blogan@psu.edu; Fax: +1-814-863-7304

Authors

Le Shi − *Department of Civil and Environmental Engineering, The Pennsylvania State University, University Park, Pennsylvania 16802, United States;* orcid.org/0000-0003-1794-1256

Evan Newcomer − *Department of Civil and Environmental Engineering, The Pennsylvania State University, University Park, Pennsylvania 16802, United States*

Moon Son − *Department of Civil and Environmental Engineering, The Pennsylvania State University, University*

https://doi.org/10.1021/acs.est.0c08629
Environ. Sci. Technol. 2021, 55, 5412−5421

Park, Pennsylvania 16802, United States; orcid.org/0000-0002-3770-148X

Vineeth Pothanamkandathil − *Department of Civil and Environmental Engineering, The Pennsylvania State University, University Park, Pennsylvania 16802, United States*

Christopher A. Gorski − *Department of Civil and Environmental Engineering, The Pennsylvania State University, University Park, Pennsylvania 16802, United States;* orcid.org/0000-0002-5363-2904

Ahmed Galal − *Chemistry Department, Faculty of Science, Cairo University, Giza 12613, Egypt;* orcid.org/0000-0001-9097-6725

Complete contact information is available at: https://pubs.acs.org/10.1021/acs.est.0c08629

Notes

The authors declare no competing financial interest.

■ ACKNOWLEDGMENTS

Funding for data presented here was provided by the USAID and NAS through Subaward 2000010557, and any opinions, findings, conclusions, or recommendations expressed in this article are those of the authors alone and do not necessarily reflect the views of USAID or NAS.

■ REFERENCES

(1) Elimelech, M.; Phillip, W. A. The future of seawater desalination: Energy, technology, and the environment. *Science* **2011**, *333*, 712−717.

(2) Strathmann, H. Electrodialysis, a mature technology with a multitude of new applications. *Desalination* **2010**, *264*, 268−288.

(3) Schlumpberger, S.; Lu, N. B.; Suss, M. E.; Bazant, M. Z. Scalable and continuous water deionization by shock electrodialysis. *Environ. Sci. Technol. Lett.* **2015**, *2*, 367−372.

(4) Kim, S. J.; Ko, S. H.; Kang, K. H.; Han, J. Direct seawater desalination by ion concentration polarization. *Nat. Nanotechnol.* **2010**, *5*, 297−301.

(5) Porada, S.; Zhao, R.; van der Wal, A.; Presser, V.; Biesheuvel, P. M. Review on the science and technology of water desalination by capacitive deionization. *Prog. Mater. Sci.* **2013**, *58*, 1388−1442.

(6) AlMarzooqi, F. A.; Al Ghaferi, A. A.; Saadat, I.; Hilal, N. Application of capacitive deionisation in water desalination: A review. *Desalination* **2014**, *342*, 3−15.

(7) Wang, L.; Zhang, C.; He, C.; Waite, T. D.; Lin, S. Equivalent film-electrode model for flow-electrode capacitive deionization: Experimental validation and performance analysis. *Water Res.* **2020**, *181*, 115917.

(8) Wang, L.; Lin, S. Theoretical framework for designing a desalination plant based on membrane capacitive deionization. *Water Res.* **2019**, *158*, 359−369.

(9) Zhang, X.; Zuo, K.; Zhang, X.; Zhang, C.; Liang, P. Selective ion separation by capacitive deionization (cdi) based technologies: A state-of-the-art review. *Environ. Sci.: Water Res. Technol.* **2020**, *6*, 243−257.

(10) Kim, T.; Gorski, C. A.; Logan, B. E. Low energy desalination using battery electrode deionization. *Environ. Sci. Technol. Lett.* **2017**, *4*, 444−449.

(11) Pothanamkandathil, V.; Fortunato, J.; Gorski, C. A. Electrochemical desalination using intercalating electrode materials: A comparison of energy demands. *Environ. Sci. Technol.* **2020**, *54*, 3653−3662.

(12) Son, M.; Pothanamkandathil, V.; Yang, W.; Vrouwenvelder, J. S.; Gorski, C. A.; Logan, B. E. Improving the thermodynamic energy efficiency of battery electrode deionization using flow-through electrodes. *Environ. Sci. Technol.* **2020**, *54*, 3628−3635.

(13) Kim, T.; Gorski, C. A.; Logan, B. E. Ammonium removal from domestic wastewater using selective battery electrodes. *Environ. Sci. Technol. Lett.* **2018**, *5*, 578−583.

(14) Wang, L.; Dykstra, J. E.; Lin, S. Energy efficiency of capacitive deionization. *Environ. Sci. Technol.* **2019**, *53*, 3366−3378.

(15) Wang, R.; Lin, S. Thermodynamic reversible cycles of electrochemical desalination with intercalation materials in symmetric and asymmetric configurations. *J. Colloid Interface Sci.* **2020**, *574*, 152−161.

(16) Hou, C.-H.; Liang, C.; Yiacoumi, S.; Dai, S.; Tsouris, C. Electrosorption capacitance of nanostructured carbon-based materials. *J. Colloid Interface Sci.* **2006**, *302*, 54−61.

(17) Suss, M. E.; Presser, V. Water desalination with energy storage electrode materials. *Joule* **2018**, *2*, 10−15.

(18) Pasta, M.; Wessells, C. D.; Cui, Y.; La Mantia, F. A desalination battery. *Nano Lett.* **2012**, *12*, 839−843.

(19) Guo, L.; Mo, R.; Shi, W.; Huang, Y.; Leong, Z. Y.; Ding, M.; Chen, F.; Yang, H. Y. A prussian blue anode for high performance electrochemical deionization promoted by the faradaic mechanism. *Nanoscale* **2017**, *9*, 13305−13312.

(20) Desai, D.; Beh, E. S.; Sahu, S.; Vedharathinam, V.; van Overmeere, Q.; de Lannoy, C. F.; Jose, A. P.; Völkel, A. R.; Rivest, J. B. Electrochemical desalination of seawater and hypersaline brines with coupled electricity storage. *ACS Energy Lett.* **2018**, *3*, 375−379.

(21) Porada, S.; Shrivastava, A.; Bukowska, P.; Biesheuvel, P. M.; Smith, K. C. Nickel hexacyanoferrate electrodes for continuous cation intercalation desalination of brackish water. *Electrochim. Acta* **2017**, *255*, 369−378.

(22) Singh, K.; Qian, Z.; Biesheuvel, P. M.; Zuilhof, H.; Porada, S.; de Smet, L. C. P. M. Nickel hexacyanoferrate electrodes for high mono/divalent ion-selectivity in capacitive deionization. *Desalination* **2020**, *481*, 114346.

(23) Lee, J.; Kim, S.; Yoon, J. Rocking chair desalination battery based on prussian blue electrodes. *ACS Omega* **2017**, *2*, 1653−1659.

(24) Zhu, X.; Xu, W.; Tan, G.; Wang, Y. Concentration flow cells for efficient salinity gradient energy recovery with nanostructured open framework hexacyanoferrate electrodes. *ChemistrySelect* **2018**, *3*, 5571−5580.

(25) Xu, Y.; Zheng, S.; Tang, H.; Guo, X.; Xue, H.; Pang, H. Prussian blue and its derivatives as electrode materials for electrochemical energy storage. *Energy Storage Mater.* **2017**, *9*, 11−30.

(26) Wang, B.; Han, Y.; Wang, X.; Bahlawane, N.; Pan, H.; Yan, M.; Jiang, Y. Prussian blue analogs for rechargeable batteries. *iScience* **2018**, *3*, 110−133.

(27) Wessells, C. D.; Peddada, S. V.; McDowell, M. T.; Huggins, R. A.; Cui, Y. The effect of insertion species on nanostructured open framework hexacyanoferrate battery electrodes. *J. Electrochem. Soc.* **2011**, *159*, A98−A103.

(28) Smith, K. C. Theoretical evaluation of electrochemical cell architectures using cation intercalation electrodes for desalination. *Electrochim. Acta* **2017**, *230*, 333−341.

(29) Yi, H.; Qin, R.; Ding, S.; Wang, Y.; Li, S.; Zhao, Q.; Pan, F. Structure and properties of prussian blue analogues in energy storage and conversion applications. *Adv. Funct. Mater.* **2020**, *31*, 2006970.

(30) Wang, R. Y.; Shyam, B.; Stone, K. H.; Weker, J. N.; Pasta, M.; Lee, H.-W.; Toney, M. F.; Cui, Y. Reversible multivalent (monovalent, divalent, trivalent) ion insertion in open framework materials. *Adv. Energy Mater.* **2015**, *5*, 1401869.

(31) Nightingale, E. R. Phenomenological theory of ion solvation. Effective radii of hydrated ions. *J. Phys. Chem.* **1959**, *63*, 1381−1387.

(32) Pasta, M.; Wessells, C. D.; Huggins, R. A.; Cui, Y. A high-rate and long cycle life aqueous electrolyte battery for grid-scale energy storage. *Nat. Commun.* **2012**, *3*, 1149.

(33) Wessells, C. D.; Huggins, R. A.; Cui, Y. Copper hexacyanoferrate battery electrodes with long cycle life and high power. *Nat. Commun.* **2011**, *2*, 550.

(34) Jiao, S.; Tuo, J.; Xie, H.; Cai, Z.; Wang, S.; Zhu, J. The electrochemical performance of $Cu_3[Fe(CN)_6]_2$ as a cathode material for sodium-ion batteries. *Mater. Res. Bull.* **2017**, *86*, 194−200.

(35) Stilwell, D. E.; Park, K. H.; Miles, M. H. Electrochemical studies of the factors influencing the cycle stability of prussian blue films. *J. Appl. Electrochem.* **1992**, *22*, 325−331.
(36) Shrivastava, A.; Liu, S.; Smith, K. C. Linking capacity loss and retention of nickel hexacyanoferrate to a two-site intercalation mechanism for aqueous Mg^{2+} and Ca^{2+} ions. *Phys. Chem. Chem. Phys.* **2019**, *21*, 20177−20188.
(37) Wei, W.; Zou, W.; Yang, D.; Zheng, R.; Wang, R.; Chen, H. A highly efficient porous conductive polymer electrode for seawater desalination. *J. Mater. Chem. A* **2020**, *8*, 11811−11817.
(38) Jiang, Y.; Liu, J. Definitions of pseudocapacitive materials: A brief review. *Energy Environ. Mater.* **2019**, *2*, 30−37.
(39) Wang, J.; Polleux, J.; Lim, J.; Dunn, B. Pseudocapacitive contributions to electrochemical energy storage in TiO_2 (anatase) nanoparticles. *J. Phys. Chem. C* **2007**, *111*, 14925−14931.
(40) Augustyn, V.; Simon, P.; Dunn, B. Pseudocapacitive oxide materials for high-rate electrochemical energy storage. *Energy Environ. Sci.* **2014**, *7*, 1597−1614.
(41) Geise, G. M.; Cassady, H. J.; Paul, D. R.; Logan, B. E.; Hickner, M. A. Specific ion effects on membrane potential and the permselectivity of ion exchange membranes. *Phys. Chem. Chem. Phys.* **2014**, *16*, 21673−21681.
(42) Luo, J.; Sam, A.; Hu, B.; DeBruler, C.; Wei, X.; Wang, W.; Liu, T. L. Unraveling ph dependent cycling stability of ferricyanide/ferrocyanide in redox flow batteries. *Nano Energy* **2017**, *42*, 215−221.
(43) Holleman, A.; Wiberg, E. *Inorganic Chemistry*; Academic Press: San Diego, 2001, ISBN 0-12-352651-5.
(44) Wang, R. Y.; Wessells, C. D.; Huggins, R. A.; Cui, Y. Highly reversible open framework nanoscale electrodes for divalent ion batteries. *Nano Lett.* **2013**, *13*, 5748−5752.
(45) Lim, J.; Kasiri, G.; Sahu, R.; Schweinar, K.; Hengge, K.; Raabe, D.; La Mantia, F.; Scheu, C. Irreversible structural changes of copper hexacyanoferrate used as a cathode in zn-ion batteries. *Chem.—Eur. J.* **2020**, *26*, 4917−4922.
(46) Kasiri, G.; Glenneberg, J.; Kun, R.; Zampardi, G.; La Mantia, F. Microstructural changes of prussian blue derivatives during cycling in zinc-containing electrolytes. *ChemElectroChem* **2020**, *7*, 3301−3310.
(47) Lee, H. J.; Kim, D. Y.; Jeong, S. K. Effect of ball milling process on electrochemical properties of copper hexacyanoferrate active material for calcium-ion batteries. *Key Eng. Mater.* **2019**, *803*, 109−114.
(48) Dykstra, J. E.; Keesman, K. J.; Biesheuvel, P. M.; van der Wal, A. Theory of ph changes in water desalination by capacitive deionization. *Water Res.* **2017**, *119*, 178−186.
(49) Zhang, D.; Yan, T.; Shi, L.; Peng, Z.; Wen, X.; Zhang, J. Enhanced capacitive deionization performance of graphene/carbon nanotube composites. *J. Mater. Chem.* **2012**, *22*, 14696−14704.
(50) Chao, D.; Zhou, W.; Xie, F.; Ye, C.; Li, H.; Jaroniec, M.; Qiao, S.-Z. Roadmap for advanced aqueous batteries: From design of materials to applications. *Sci. Adv.* **2020**, *6*, No. eaba4098.
(51) Giurg, A.; Denk, K.; Bystron, T.; Paidar, M.; Bouzek, K. Electrode degradation mechanisms in capacitive deionisation. *Desalination* **2021**, *497*, 114622.
(52) Yu, M.; Lu, Y.; Zheng, H.; Lu, X. New insights into the operating voltage of aqueous supercapacitors. *Chem.—Eur. J.* **2018**, *24*, 3639−3649.
(53) Guduru, R.; Icaza, J. A brief review on multivalent intercalation batteries with aqueous electrolytes. *Nanomaterials* **2016**, *6*, 41.
(54) Gu, X.; Liu, J.-l.; Yang, J.-h.; Xiang, H.-j.; Gong, X.-g.; Xia, Y.-y. First-Principles Study of H+ Intercalation in Layer-Structured LiCoO2. *J. Phys. Chem. C* **2011**, *115*, 12672−12676.
(55) Yang, X.; Rogach, A. L. Electrochemical techniques in battery research: A tutorial for nonelectrochemists. *Adv. Energy Mater.* **2019**, *9*, 1900747.
(56) Dong, X.; Yang, Y.; Wang, B.; Cao, Y.; Wang, N.; Li, P.; Wang, Y.; Xia, Y. Low-Temperature Charge/Discharge of Rechargeable Battery Realized by Intercalation Pseudocapacitive Behavior. *Adv. Sci.* **2020**, *7*, 2000196.
(57) Huo, S.; Song, X.; Zhao, Y.; Ni, W.; Wang, H.; Li, K. Insight into the significant contribution of intrinsic carbon defects for the high-performance capacitive desalination of brackish water. *J. Mater. Chem. A* **2020**, *8*, 19927−19937.
(58) Du, X.; Hao, X.; Wang, Z.; Guan, G. Electroactive ion exchange materials: Current status in synthesis, applications and future prospects. *J. Mater. Chem. A* **2016**, *4*, 6236−6258.
(59) Li, C. H.; Peprah, M. K.; Asakura, D.; Meisel, M. W.; Okubo, M.; Talham, D. R. Stepwise Reduction of Electrochemically Lithiated Core-Shell Heterostructures Based on the Prussian Blue Analogue Coordination Polymers K0.1Cu[Fe(CN)6]0.7·3.5H2O and K0.1Ni-[Fe(CN)6]0.7·4.4H2O. *Chem. Mater.* **2015**, *27*, 1524−1530.
(60) Xu, Y.; Wan, J.; Huang, L.; Xu, J.; Ou, M.; Liu, Y.; Sun, X.; Li, S.; Fang, C.; Li, Q.; Han, J.; Huang, Y.; Zhao, Y. Dual redox-active copper hexacyanoferrate nanosheets as cathode materials for advanced sodium-ion batteries. *Energy Storage Mater.* **2020**, *33*, 432−441.
(61) Giorgetti, M.; Guadagnini, L.; Tonelli, D.; Minicucci, M.; Aquilanti, G. Structural characterization of electrodeposited copper hexacyanoferrate films by using a spectroscopic multi-technique approach. *Phys. Chem. Chem. Phys.* **2012**, *14*, 5527−5537.
(62) Kuperman, N.; Cairns, A.; Goncher, G.; Solanki, R. Structural water enhanced intercalation of magnesium ions in copper hexacyanoferrate nonaqueous batteries. *Electrochim. Acta* **2020**, *362*, 137077.
(63) Mullaliu, A.; Aquilanti, G.; Conti, P.; Plaisier, J. R.; Fehse, M.; Stievano, L.; Giorgetti, M. Copper electroactivity in prussian blue-based cathode disclosed by operando XAS. *J. Phys. Chem. C* **2018**, *122*, 15868−15877.
(64) Makowski, O.; Stroka, J.; Kulesza, P. J.; Malik, M. A.; Galus, Z. Electrochemical identity of copper hexacyanoferrate in the solid-state: Evidence for the presence and redox activity of both iron and copper ionic sites. *J. Electroanal. Chem.* **2002**, *532*, 157−164.
(65) Guo, J.; Ming, J.; Lei, Y.; Zhang, W.; Xia, C.; Cui, Y.; Alshareef, H. N. Artificial solid electrolyte interphase for suppressing surface reactions and cathode dissolution in aqueous zinc ion batteries. *ACS Energy Lett.* **2019**, *4*, 2776−2781.

https://doi.org/10.1021/acs.est.0c08629
Environ. Sci. Technol. 2021, 55, 5412−5421